Corrosion Science 169 (2020) 108607

Contents lists available at ScienceDirect

Corrosion Science

journal homepage: www.elsevier.com/locate/corsci

The influence of sulphide, bicarbonate and carbonate on the electrochemistry of carbon steel in slightly alkaline solutions

Maxwell Goldman[a], Claire Tully[a], James J. Noël[a,b], David W. Shoesmith[a,b,*]

[a] Department of Chemistry, the University of Western Ontario, London, Ontario, N6A 5B7 Canada
[b] Surface Science Western, 999 Collip Circle, London, Ontario, N6G 0J3, Canada

ARTICLE INFO

Keywords:
Carbon steel
Alkaline corrosion
Passivity
Cyclic voltammetry
Raman spectroscopy

ABSTRACT

The influence of sulphide on the electrochemistry of carbon steel in neutral to slightly alkaline sulphide solutions was investigated using electrochemical and surface analytical techniques. Small concentrations of sulphide were found to promote anodic dissolution as Fe^{II} carbonate complexes and to destabilize Fe^{III} oxides leading to the loss of passivity, especially at pH ≤ 9. The dominant phase formed was mackinawite, while reactions between Fe^{III} and sulphide led to the formation of oxidized S species (elemental S and sulphate), polysulfides, and pyrite.

1. Introduction

Internal and external corrosion of transmission pipelines are costly issues in the oil and gas industry. Internal corrosion is dictated by the composition of the gas or oil being transported, which can lead to acidic, sweet, or sour corrosion [1]. External corrosion remains an ongoing concern for the structural integrity of Canadian pipelines [2], with corrosion generally occurring when pipeline coatings disbond, exposing the steel to groundwater and shielding it from cathodic protection. Groundwaters to which pipelines will be exposed are commonly near neutral to slightly alkaline and contain bicarbonate/carbonate, sulphate and chloride anions. When anaerobic conditions prevail, the steel becomes susceptible to microbially-induced corrosion (MIC) when sulphate-reducing bacteria (SRB), organisms commonly encountered in the soils surrounding the buried pipelines, are present. SRBs are facultative anaerobes that utilize sulphate (SO_4^{2-}) as a terminal electron acceptor during energy generation, to produce SH- as one of the byproducts of the cathodic reaction [3],

$$SO_4^{2-} + 9H^+ + 8e- \rightarrow SH- + 4H_2O \quad (1)$$

Recent studies on the corrosion products formed electrochemically on carbon steel in the slightly alkaline groundwaters anticipated to contact pipelines show magnetite (Fe_3O_4) and maghemite (γ-Fe_2O_3) to be the kinetically-favoured oxides formed between -800 mV (vs. SCE) and -600 mV (vs. SCE) and at potentials > -500 mV (vs. SCE), respectively [4,5]. When additional anions are present (such as carbonate, chloride and sulphide), considerably more complex behavior is anticipated with possible corrosion products, including various iron carbonates, iron sulphides, and iron chlorides [6–9]. Previous studies have attempted to determine the relative influence of anions on the kinetics of the anodic reactions occurring on the steel [10–13].

The sulphide produced by MIC is aggressive and can accelerate corrosion of the steel. When sulphide is present, iron sulphides become the dominant corrosion product with the composition and protective nature of the product dependent on pH, temperature and sulphide concentration [14]. At low pH (< 2) iron undergoes active dissolution and thus no iron sulphide is formed [14–16]. At higher pH values (< 7) and in the presence of sulphides, the initial film formed is mackinawite (FeS_{1-x}: $0 < x < 0.11$) which can lead to the suppression of corrosion by transformation into more compact iron sulphide phases such as troilite (FeS) [15,17] and pyrrhotite ($Fe_{1-x}S$: $0 < x < 0.2$) [14].

The concentration of sulphide is also important in determining the protectiveness of the iron sulphide film, with films formed at lower sulphide concentrations being more protective than those formed at higher concentrations due to the difference in film porosity [18]. In alkaline solutions, mackinawite is the phase commonly formed and can remain protective, providing it remains intact and does not fracture [19,20]. Previous work has also been reported that mackinawite formation can lead to pitting in alkaline solutions possibly due to a competition between oxide and sulphide film formation [19–22].

In this study, the role of sulphide, carbonate, and bicarbonate on the formation of iron oxide and iron sulphide films in near-neutral to alkaline conditions has been studied using electrochemical and surface analytical techniques. The primary goal of the study was to determine the relative influence of prominent anions found in groundwater in controlling the formation of iron oxides and iron sulphides over the pH

* Corresponding author.
E-mail address: dwshoesm@uwo.ca (D.W. Shoesmith).

https://doi.org/10.1016/j.corsci.2020.108607
Received 18 November 2019; Received in revised form 10 March 2020; Accepted 14 March 2020
Available online 18 March 2020
0010-938X/

range from 8–10, the likely range to be encountered on the external surfaces of Canadian oil and gas pipelines [19,20,23,24].

2. Experimental

2.1. Materials and electrode preparation

Experiments were performed using A516 Grade 70 carbon steel (0.0070 P; 0.0030 O; 0.0040 Mo; 0.010 S; 0.01 Cu; 0.010 Ni; 0.019 V; 0.020 Cr; 0.036 Al; 0.23 C; 0.26 Si; 1.1 Mn (μg g^{-1})) rotating disk electrodes (RDE). The RDE was fixed in a Teflon holder using epoxy resin, with the back threaded with a stainless-steel rod to provide contact to external circuitry. For static experiments, the electrode was set into epoxy resin, and the stainless-steel shaft covered with Teflon shrink tubing. The exposed electrode surface area was 0.79 cm^2 for both RDE and static electrodes. Pre-experiment the surface was polished with SiC papers up to P1200. Each electrode was rinsed with Type 1 water (resistivity of 18.2 MΩ.cm) and dried using argon gas flow. Prior to an experiment, all electrodes were cathodically cleaned for 1 min (to remove air-formed oxide) at -1.3 V vs. saturated calomel electrode (SCE) and -1.1 V vs. SCE (to allow the detachment of cathodically formed H_2 bubbles).

2.2. Solution preparation

Solutions were prepared with Type 1 water, using reagent grade chemicals (Na_2S Sigma Aldrich: Na_2CO_3 and $NaHCO_3$ from Caledon Laboratories). The base carbonate solution of 0.1 M sodium bicarbonate and 0.1 M sodium carbonate solution was argon sparged before the addition of sulphide and throughout the experiment. The sulphide solution was prepared by sparging Type 1 water with argon gas before adding sulphide. The sulphide solution was added to the carbonate solution to the desired sulphide concentration, in these experimented three sulphide concentrations were between 10^{-6} M and 10^{-3} M. All experiments were carried out at pH values in the range of 8–10, with the pH adjusted using H_2SO_4. All cyclic voltammograms, potentiodynamic scans, and potentiostatic experiments were run in deareated conditions, achieved by continuously purging with argon gas.

2.3. Electrochemical setup & techniques

All experiments were carried out in a standard three-electrode electrochemical glass cell, with a platinum sheet as the counter electrode and a standard calomel reference electrode (SCE (0.242 V vs. saturated hydrogen electrode)). The rotation rate of the RDE working electrode (10 Hz) was controlled by a Pine Instrument Company Analytical Rotator Model AFA86 Serial 882, and electrochemical measurements were performed using a 1287 Solartron Potentiostat or a 1480 Solartron MultiStat. CorrWare software was used to control experiments and to collect electrochemical data.

CV experiments commenced at -1.1 V vs. SCE with the potential scanned at 7.00 mV/s to either −0.4 V or -0.3 V (vs. SCE). Potentiostatic experiments were performed at a potential of −0.55 V (vs. SCE) for 1 h. Potentiodynamic scans (PDS) were carried out in an anaerobic chamber. The potential was scanned from −1.1 V (vs. SCE) to -0.4 V (vs. SCE) at a scan rate of 1.95 mV/s. The surfaces of the steel electrodes after PDS experiments were analyzed by scanning electron microscopy (SEM), energy dispersive X-ray (EDX) analysis, X-ray photoelectron spectroscopy (XPS), and Raman spectroscopy. To minimize atmospheric exposure, the electrochemical cell was placed in a glovebox before the electrode was extracted. Samples were transferred from the glovebox into the X-ray photoelectron spectrometer in an argon sparged (1.5 h) glovebag via a vacuum transfer vessel. Afterwards samples were briefly exposed to air prior to SEM/EDX analysis and Raman spectroscopy.

2.4. Surface analytical techniques

2.4.1. X-ray photoelectron spectroscopy

XPS experiments were conducted on a Kratos AXIS Ultra Spectrometer using a monochromatic Al Kα (15 mA, 14 kV) radiation source ($h\nu$ = 1486.6 eV). The Au $4f_{7/2}$ metallic Au binding energy (83.95 eV) was used as a reference point for calibration of the instrument work function. When required, spectra were corrected for charging by setting the C−C peak in the C 1s spectrum to 284.8 eV. Survey spectra and high-resolution spectra were recorded for the Fe 2p, S 2p, C 1s, and O 1s spectral regions. Spectra were analyzed using CasaXPS® software, which incorporated a Shirley background correction.

2.4.2. Scanning Electron microscopy and elemental analysis

SEM/EDX analysis was carried out using a Hitachi SU3500 Variable Pressure SEM combined with an Oxford Aztec X-Max50 SDD X-ray analyzer. All SEM/EDX analyses were carried out using an accelerating voltage of 1 keV or 10 keV.

2.4.3. Raman spectroscopy

Raman spectra were obtained using a Renishaw 2000 Raman spectrometer equipped with a 633 nm He-Ne laser and an Olympus microscope. Images were collected using a x50 uncoated objective lens with the beam focused to a diameter of ~2 μm. The power of the laser beam at the sample surface was kept to 1% to avoid laser heating effects. All spectra were calibrated against the 520.5 cm^{-1} peak of Si. GRAMS 386 Raman software was used both to collect and manipulate the spectra.

3. Results and discussion

3.1. Effect of Bicarbonate/Carbonate in the absence of sulphide

Fig. 1 shows CVs recorded in bicarbonate/carbonate (HCO_3^-/CO_3^{2-}) solutions at pH 8, 9, and 10. Based on previously published information, three potential regions, numbered in the figure, can be defined [13]. A shallow oxidation process is observed in the potential range -0.92 V to -0.75 V (depending on pH), involving the formation of an Fe^I surface intermediate and leading to the formation of $Fe(OH)_2$ through the following reactions [25,26]

$$Fe + OH^- \rightarrow FeOH^-_{ads} \quad (2)$$

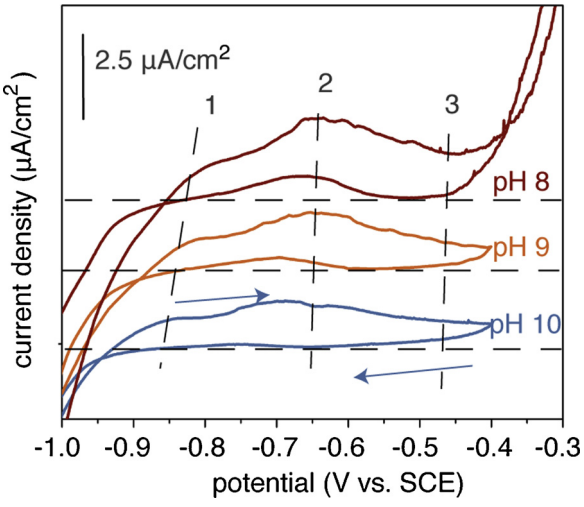

Fig. 1. Cyclic voltammograms recorded on carbon steel in a 0.2 M CO_3^{2-}/HCO_3- solution from -1.1 V to various anodic limits at a scan rate of 7 mV/s: Horizontal dashed lines indicate the baseline for each CV. Vertical dashed lines indicate regions 1, 2 and 3. Arrows indicate the scan directions.

$$FeOH^-_{ads} \rightarrow FeOH_{ads} + e^- \quad (3)$$

$$FeOH_{ads} \rightarrow FeOH^+_{ads} + e^- \quad (4)$$

$$FeOH^+_{ads} + OH^- \rightarrow Fe(OH)_2 \quad (5)$$

In region 2, (~ -0.8 V to ~ -0.6 V (vs. SCE)) the increased current, which varied with pH, can be attributed to the dissolution of Fe^{2+} by complexation with HCO_3^- [25,26],

$$Fe(OH)_2 + HCO_3^- \rightarrow FeHCO_3^+ + 2OH^- \quad (6)$$

although it is possible HCO_3^- displaces OH^- in surface coordinated species prior to dissolution. In region 3, the current decreases due to the formation of an Fe^{III}oxide (γ-Fe_2O_3) expected to passivate the steel [5]. Over the pH range investigated, the solubility's of Fe^{2+} and Fe^{3+} respond inversely, that of Fe^{2+} decreasing while that of Fe^{3+} increases, from pH 8 to pH 10 [5]. The balance between these two contrasting influences leads to a slightly increased current in region 3 as the pH decreases. That the Fe^{III}oxide is slightly less passivating at a pH of 8 is demonstrated by the increased current indicating film breakdown when the positive potential limit is extended to -0.3 V. Although not shown, such a breakdown is not observed at the two higher pH values.

3.2. The effect of sulphide

Fig. 2 shows the influence of a small addition of sulphide (10^{-5} M) has an identifiable effect on the electrochemical behaviour. Regions 1, 2, and 3 correspond to those defined in Fig. 1. In region 1, any influence on the behaviour appears marginal, although the suppression of the negative current at potentials (E) < -1.0 V indicates an inhibition of water reduction (to H_2) when sulphide is introduced. The current in region 2 is markedly increased suggesting a catalytic role of sulphide in the anodic dissolution process. A possible sequence of reactions would start with the partial displacement of OH_{ads}- by sulphide,

$$SH^- + FeOH_{ads}{}^- \rightarrow FeSH_{ads}{}^- + OH^- \quad (7)$$

followed by Fe oxidation and dissolution as $FeHCO_3^+$,

$$FeSH_{ads}{}^- \rightarrow FeSH_{ads} + e^- \quad (8)$$

$$FeSH_{ads} + HCO_3^- \rightarrow FeHCO_3^+ + SH^- + e^- \quad (9)$$

In region 3 the current decrease can be attributed to the

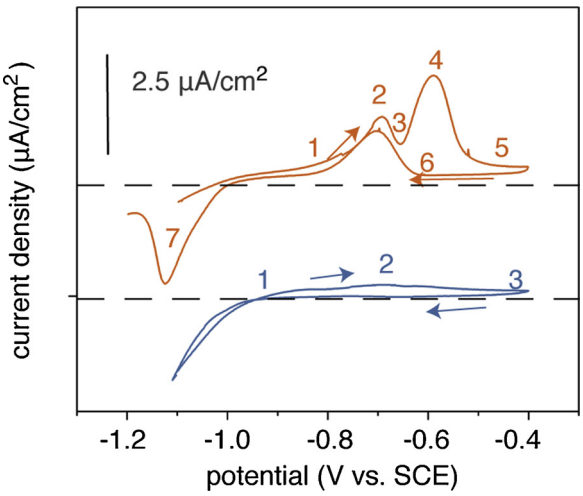

Fig. 2. Cyclic voltammograms recorded on carbon steel in a 0.2 M CO_3^{2-}/HCO_3- solution (pH 10) from -1.1 V to -0.4 V at a scan rate of 7 mV/s (blue); 0.2 M CO_3^{2-}/HCO_3-, pH 10, 10^{-5} M [SH-], from -1.1 V to -0.4 V at a scan rate of 7 mV/s (orange). Horizontal dashed lines indicate the baselines. Arrows indicate direction of the scan. (For interpretation of the references to colour in this figure legend, the reader is referred to the web version of this article).

transformation of $Fe(OH)_2$ to Fe_3O_4 followed by a further potential-dependent transformation to γ-Fe_2O_3,

$$Fe(OH)_2 \rightarrow Fe_3O_4 \rightarrow \gamma\text{-}Fe_2O_3 \quad (10)$$

According to Buchler et al. [27] the composition of the passive film can be considered to be $Fe^{II}_{1-x}Fe^{III}_2O_{4-x}$ with x increasing as the applied potential is increased. Such a gradual transition between Fe_3O_4 (x = 0) and γ-Fe_2O_3 (x = 1) is feasible since both oxides exhibit a cubic oxygen lattice [28].

The oxide transformation sequence (reaction (10)) to yield a passivating γ-Fe_2O_3 layer is arrested, leading to a large anodic peak (region 4) before passivation is re-enforced in region 5. Fe^{III} oxides and oxyhydroxides have been shown to be unstable in the presence of sulphide with the reaction proceeding as a surface-controlled process involving the adsorption of sulphide at Fe^{III} on the oxide surface sites [29,30],

$$Fe^{III} + SH^- \rightarrow Fe^{III}S_{ads}{}^- + H^+ \quad (11)$$

leading to electron transfer to yield an Fe^{II} surface radical species,

$$Fe^{III}S_{ads}{}^- \rightarrow Fe^{II}S^{\bullet} \quad (12)$$

followed by the release of Fe^{2+} and the $S^{\bullet -}$ radical, with Fe^{2+} release facilitated by HCO_3- complexation in the present case.

$$Fe^{II}S^{\bullet} + HCO_3^- \rightarrow FeHCO_3^+ + S^{\bullet -} \quad (13)$$

The $S^{\bullet -}$ then reacts further with Fe^{III} surface sites leading to more oxidized S species such as elemental S although further oxidation, eventually to SO_4^{2-}, has been claimed [29].

$$S^{\bullet -} + 7Fe^{III} \rightarrow SO_4^{2-} + 7Fe^{2+} \quad (14)$$

Assuming SH^- oxidation only proceeds to S, the overall reaction for γ-Fe_2O_3 can be written,

$$\gamma\text{-}Fe_2O_3 + SH^- + 2H_2O \rightarrow 2FeSH^+ + S + 5OH^- \quad (15)$$

since this sequence of reactions is chemical, not electrochemical, the revived current in region 4 (Fig. 2) must be attributed to the further anodic oxidation of the steel substrate re-exposed by the removal of the anodically forming γ-Fe_2O_3 layer. This reaction would proceed by the re-adsorption of sulphide to yield $FeSH^-_{ads}$ and the re-occurrence of reactions 8 and 9. In the presence of a significant sulphide concentration, dissolved $FeHCO_3^+$ would rapidly form insoluble FeS,

$$FeHCO_3^+ + SH^- \rightarrow FeS + HCO_3^- + H^+ \quad (16)$$

leading to the deposition of FeS on the activated surface and a decrease in the local pH. The formation of an FeS surface film would account for the reduction process in region 7 on the reverse voltammetric scan. The close equivalence of the charges associated with peaks 4 and 7 indicates that a large majority of the Fe^{2+} produced anodically in region 4 is deposited as FeS, which is then subsequently reduced in region 7.

The possibility that the FeS layer leads to the passivation of the steel indicated by the decrease in current in region 5 can be dismissed since reactivation of the steel is observed on the reverse scan in region 6 prior to the removal of the FeS deposit in region 7. This indicates that passivation is enforced by the enhancement of the oxide transformation sequence (reaction (10)) when the potential is increased into region 5. As the potential is increased, the rate of formation of Fe^{III} (as oxide) will be increased while the rate of its chemical reduction by SH^- will be unbiased by potential. On the reverse scan, the decreased rate of Fe^{III} formation eventually cannot compensate for its chemical destruction by the overall reaction (15), and active conditions are reestablished in region 6. The inability of the deposited FeS to enforce passivation of the surface is consistent with expectations for sulphide films. Similar studies on copper showed sulphide films to be porous and not passive [31].

Fig. 3 shows CVs recorded at the three pH values in solutions containing different sulphide concentrations. At a pH of 10 (Fig. 3(a)) the

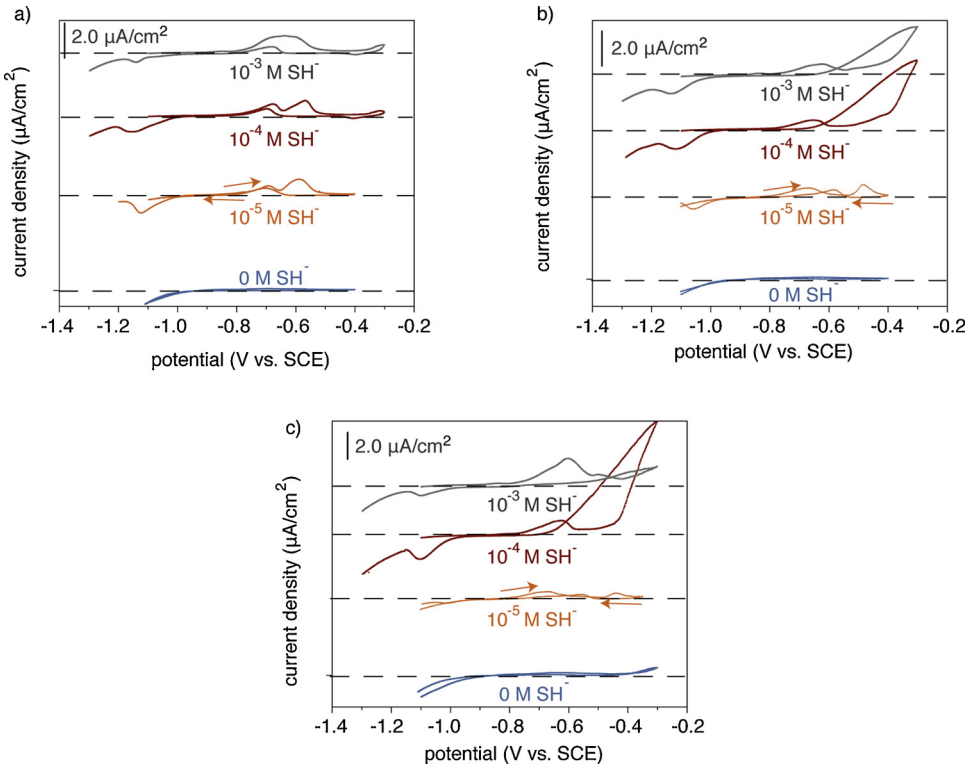

Fig. 3. Cyclic voltammograms recorded on carbon steel in a 0.2 M CO_3^{2-}/HCO_3- solution from -1.1 V to either -0.4 V or -0.3 V at a scan rate of 7 mV/s for various [SH-]: (a) pH 10; (b) pH 9; (c) pH 8. Horizontal dashed lines indicate the baseline. Arrows show the scan direction.

anodic regions (defined in Fig. 2) are distinct at the two lower sulphide concentrations. At a sulphide concentration of 10^{-3} M, the current decrease associated with region 3 is not observed. The increased current in region 2 could be due to the extensive displacement of $OH\text{-}_{ads}$ by $SH\text{-}_{ads}$ on the steel surface leading to the accelerated dissolution of Fe^{2+} via the reaction sequence 8 and 9, and possibly the deposition of FeS if local Fe^{2+} concentrations are high enough. The disappearance of the distinct separation of anodic peaks 2 and 4 is consistent with an increase in the rate of chemical reduction of Fe^{III} via the reaction sequence (11) to (14) which would be expected to be strongly dependent on sulphide concentration and to commence as soon as Fe^{III} surface states begin to form. Despite this enhanced reaction rate, passivation due to the formation of Fe^{III} oxide is re-enforced at sufficiently positive potentials. This is to be expected since calculations of the dominant solution species show Fe^{2+} hydroxyl complexes $Fe(OH)_3$- would be dominant for a pH greater than 9 [32]. While the extent of Fe^{2+} formation increases with sulphide concentration, as indicated by the increased anodic charge associated with the potential region encompassing peaks 2 and 4 (Fig. 2), the peak for the reduction of FeS (region 7) decreases in size. This indicates that the FeS, which forms due to the production of Fe^{2+}, is likely precipitated as detached particulates and hence not completely electrochemically detectable on the reverse scan.

Although passivity is enforced, the current in the passive region 5 (defined in Fig. 2) increased as sulphide concentration increased. This behaviour is consistent with a competition between the electrochemical formation of a passivating Fe^{III} oxide and its destruction by chemical reaction with sulphide. To determine whether this would lead to the eventual breakdown of the passive oxide, the scans at the two higher sulphide concentrations were extended to −0.3 V vs. SCE. Minor anodic oxidation coupled to a cathodic reduction on the reverse scan is observed in the potential range −0.4 V to -0.3 V. Present understanding is that the oxide transformation, reaction (9), leads to a bilayer consisting of inner Fe_3O_4 and outer γ-Fe_2O_3 layers [33–35]. Consequently, the anodic process occurring in this potential region can be attributed to the conversion of the inner Fe_3O_4 layer to γ-FeOOH, a process that leads to the development of stresses in the oxide [5] and the breakdown of the film when aggressive anions are present [36].

While the enhanced anodic current does not lead to a major film breakdown, the observation of a slightly negative current on the reverse scan demonstrates the presence of reducible oxidized species formed on the forward scan. Since the film restructuring has been attributed to the conversion of an Fe_3O_4 sublayer, the reduction of the Fe^{III} states formed electrochemically will be retained at the electrode surface, allowing them to be reduced on the reverse scan.

The increase in anodic current in region 2 for reactions (8) and (9) would be expected to lead to an increase in the deposition of FeS via reaction (16). However, the peak for the reduction of FeS in region 7 decreases as the anodic current increases. This suggests that the FeS, which would inevitably have formed, does not collect on the steel surface in a morphology that enables the electron transfer for its cathodic reduction. That reducible FeS is collected when formed at low sulphide concentrations (Figs. 2 and 3(a)) but not at high sulphide concentrations, suggests a change in either the mechanism of FeS formation or in the morphology of the FeS surface deposit.

At the two lower pH values the separation between the two anodic processes in regions 2 and 4 is less readily distinguished and a major film breakdown is observed when the potential is scanned into region 5 where conversion of the inner Fe_3O_4 layer of the passive oxide occurs, Fig. 3(b) and (c). Both of these features, in particular, the breakdown as a consequence of film conversion, are facilitated by the loss of buffering capacity by the HCO_3^-/CO_3^{2-} equilibrium for which the pK_a is 10.3. As a consequence, the destruction of oxide by reaction with sulphide, which leads to the production of protons, reaction (11), will cause a decrease in pH facilitating oxide film breakdown in region 5. In this potential region the direct anodic formation of soluble Fe^{3+} and its hydrolysis to $Fe(OH)_x^{(3-x)-}$ could also occur enhancing local acidity and inhibiting passive film formation. As observed at a pH of 10, the peak for FeS reduction in region 7 decreases as sulphide concentration increases and the current for Fe^{2+} formation increases.

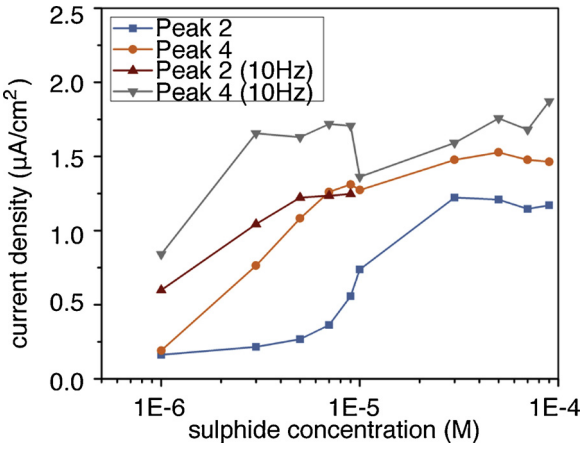

Fig. 4. Current values measured on carbon steel for peak 2 and peak 4 in cyclic voltammograms recorded at 0 Hz and 10 Hz in a 0.2 M HCO_3^-/CO_3^{2-} solution (pH 10) as a function of [SH^-].

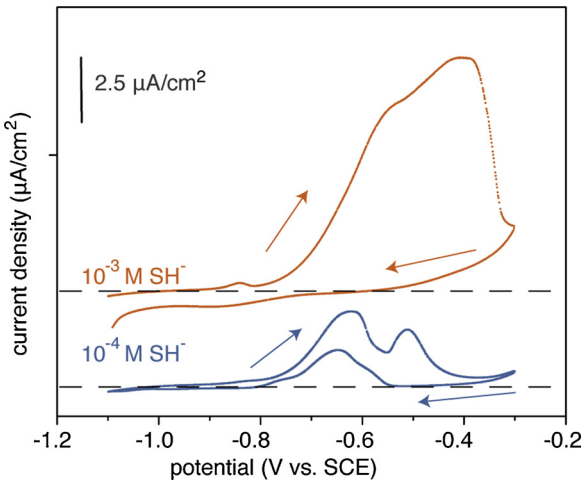

Fig. 5. Cyclic voltammograms of steel in 0.2 M CO_3^{2-}/HCO_3- from -1.1 V to -0.3 V at a scan rate of 7 mV/s at pH 8 and rotating at a rate of 10 Hz in the presence of: 10^{-4} M [SH-] (blue); 10^{-3} M [SH-] (orange). Horizontal dashed lines indicate 0 current for each CV. Arrows indicate the scan direction for the CVs. (For interpretation of the references to colour in this figure legend, the reader is referred to the web version of this article).

3.3. Influence of electrode rotation

Fig. 4 shows the influence of electrode rotation rate on the current values associated with the anodic peaks in regions 2 and 4 (Fig. 2) as a function of sulphide concentration at a pH of 10. The data set is confined to sulphide concentrations below 10^{-4} M when the current peaks in these regions can be distinguished. Under stagnant conditions, the current associated with reactions in region 2 (labeled peak 2 in the figure) is only marginally influenced at sulphide concentrations equal or greater than 5×10^{-6} M but significantly increases over the higher concentration range up to $\sim 2 \times 10^{-5}$ M beyond which the current stabilizes. This behaviour indicates a minimal influence of sulphide at low concentrations followed by the displacement of OH_{ads}- by SH_{ads}- as sulphide concentration is increased, leading to the onset of sulphide-catalyzed anodic dissolution via reactions (8) and (9). When the electrode is rotated, the current in the low sulphide concentration range increases markedly, demonstrating that the displacement of OH_{ads}- by SH_{ads}- is controlled by the flux of sulphide to the steel surface. Since the pH is close to the pK_a for the HCO_3-/CO_3^{2-} equilibrium and $[CO_3]_{tot}$ (= [HCO_3-] + [CO_3^{2-}]) > > [SH-], the flux of HCO_3-/CO_3^{2-} would not be expected to have a significant influence on the anodic current.

The current associated with region 4 (labelled peak 4 in the figure) increases linearly with sulphide concentration, indicating a dependence on concentration consistent with the expectations for the chemical reaction sequence (11) to (13). For a sulphide concentration greater or equal to 10^{-5} M, the current becomes independent of the concentration suggesting the overall rate of reactions (11) to (13) becomes controlled by other processes such as the rate of development of the passivating γ-Fe_2O_3 layer. The influence of electrode rotation rate at low sulphide concentrations shows the reaction exhibits partial control by sulphide transport.

At the lower pH values (8 and 9), when pH is significantly less than the pK_a, the influence of rotation rate is to increase the currents markedly, a feature that can be attributed to local acidification in the absence of buffering. Fig. 5 shows CVs recorded at pH 9 and an electrode rotation rate of 10 Hz in solutions containing 10^{-4} M and 10^{-3} M sulphide. Comparison to the scans in the same solutions under stagnant conditions (Fig. 2(b)) demonstrates the influence of electrode rotation rate. Similar behavior (not shown) is observed at pH 8, with the separation between peaks 2 and 4 being re-established at the lower sulphide concentrations and film breakdown being avoided in region 5. At the higher sulphide concentrations, the anodic currents in regions 2 and 4 are substantially increased but eventually suppressed by partial repassivation. In addition, despite the very large anodic currents, which at high sulphide concentrations would be expected to lead to the copious formation of FeS, the FeS reduction peak in region 7 is effectively eliminated. This supports the argument that any FeS formed is detached from the steel.

3.4. Influence of carbonate and bicarbonate

Fig. 6 shows the influence of $[CO_3]_{tot}$ on the current densities and peak potentials in regions 2, 4, and 5 (at -0.4 V (vs. SCE)). These values were recorded at pH 8 in the presence of 10^{-5} M of sulphide, when HCO_3- would be the dominant carbonate species present. As $[CO_3]_{tot}$ is increased, the current for peak 2 increases with the peak position (potential) changing only slightly, while peak 4 shifts to more positive potentials with the peak current decreasing. The current at -0.4 V (vs. SCE) increases with [HCO_3-] but not consistently.

The enhancement of the anodic current for peak 2 is consistent with the acceleration of the dissolution reaction (6) as [HCO_3^-] increases. Such an acceleration would impede the oxide transformation sequence, reaction (10), involving the surface oxidation of Fe^{II} to Fe^{III}. This acceleration of Fe^{2+} release and retardation of Fe^{III} formation would then lead to a decrease in the rate of the reaction sequence (10) to (13) accounting for the decrease in the current for peak 4 and its shift to more positive potentials. Subsequently, the combination of enhanced Fe^{2+} release and Fe^{III} reduction by sulphide would make the establishment of passivity by γ-Fe_2O_3 more difficult to achieve accounting for the current increase in region 5.

3.5. Surface analysis after potentiodynamic scans

PDS were performed in an anaerobic chamber in 0.2 M CO_3^{2-}/HCO_3- solution containing various sulphide concentrations, at pH values of 8, 9, and 10. On completion of the scans XPS, SEM/EDX, and Raman spectroscopy were performed on the electrode surfaces to elucidate the film composition, thickness, and morphology.

3.5.1. Raman spectroscopy

Freshly precipitated mackinawite is commonly nanocrystalline [37,38] as reported in the literature for amorphous FeS in anoxic sediments [39] and rust layers on steel corroded in seawater [40]. In Raman spectra for nanocrystalline mackinawite, a peak in the spectrum at 281 cm^{-1} can be attributed to the symmetric stretching mode of FeS and one at 208 cm^{-1} to a lattice mode [41]. According to Bourdoiseau

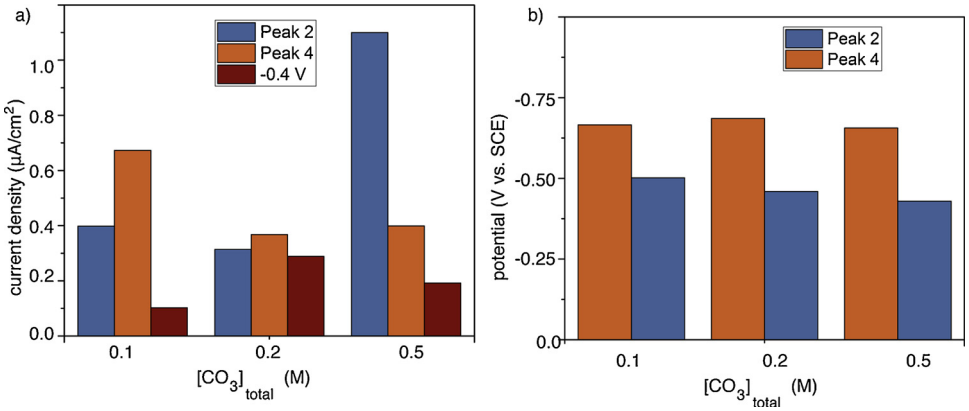

Fig. 6. a) Current densities, b) peak positions recorded in potentiodynamic scans on carbon steel in a 10^{-5} M [SH-] (pH 8) solution containing various $[CO_3]_{tot}$.

et al. [37] the conversion of nanocrystalline mackinawite to either a crystalline or partially oxidized version depends on the Fe^{2+}/SH- concentration ratio, the aging conditions (anoxic or aerated), and the drying time. If the ratio is low, then even long-term aging leads to little change in the spectrum. If the ratio is high ($3 \geq Fe/S \geq 1$), the 281 cm^{-1} peak shifts to 298 cm^{-1}. This indicates an increase in vibrational energy that correlates with the decreased lattice spacing as the Fe-S bond strengthens with crystallization, with the latter confirmed by XRD. Crystalline FeS is characterized by the intense peak at 298 cm^{-1} and two smaller peaks at 208 cm^{-1} and 257 cm^{-1}, with the first peak corresponding to the FeS stretching mode and the other two to lattice modes.

After anodic formation of FeS, XRD shows that the mackinawite formed exhibits a degree of preferred orientation with enhanced 001 diffraction peaks observed at short times which are considerably less pronounced at longer times. This loss of preferred orientation may be a consequence of the aging of the mackinawite which leads to a lattice contraction [37]. This, and the high Pilling-Bedworth ratio for FeS, would then account for the poor adhesion of the FeS to the steel surface and its ready spallation.

Mackinawite is known to be sensitive to oxidation in air leading to the formation of partially oxidized mackinawite, which is characterized by a shift in the main peak (281 cm^{-1}) to ~311 cm^{-1}, the development of a peak at 355 cm^{-1}, and the disappearance of the peak at 204 - 208 cm^{-1}. The presence of partially oxidized mackinawite usually is accompanied by other oxidized Fe species such as: greigite; magnetite; Fe^{III}oxyhydroxides, and elemental sulpur [42–45]. In addition, Mossbauer studies and XPS analyses have detected the presence of Fe^{III} within, and on the surface of, synthetic mackinawite, in either tetrahedral sites, as replacements for Fe^{II}, or in octahedral holes [46]. The incorporation of Fe^{III} within, or on the surface of, mackinawite is possibly the first stage of the oxidation process that leads to greigite, magnetite or Fe^{III}oxyhydroxides.

Fig. 7 shows the Raman spectra recorded on the electrode surfaces after PDS up to -0.4 V vs. SCE in a solution containing 0.2 M HCO_3^-/CO_3^{2-} and 10^{-3} M of sulphide. At all three pH values the spectra exhibit the bands at 311 cm^{-1} and a shoulder at 355 cm^{-1} indicating partially oxidized mackinawite and the peak at 256 cm^{-1} indicative of crystalline mackinawite. At pH 10, Fig. 7(a), the small peak at 206 cm^{-1} and the shoulder at 294 cm^{-1}, associated with nanocrystalline mackinawite, are also present. The Raman band at 472 - 482 cm^{-1} can be attributed to elemental sulphur with the small peak at 200 cm^{-1} (pH 8, Fig. 7(a)) also attributable to sulphur, and the broad band in the region 620 to 750 cm^{-1} to a mixture of Fe_3O_4 (666 cm^{-1}) and γ-Fe_2O_3 (678 cm^{-1}, 710 cm^{-1}).

While the presence of sulphur could be attributed to the chemical reaction sequence summarized in reaction (15), the observance of Fe^{III} oxides and the presence of partially oxidized mackinawite raise the possibility that air-oxidation of mackinawite occurred during the electrode analyses, despite the precautions taken to avoid it. Alternatively, Fe^{III} oxides could have been formed via an electrochemical route at the exposed steel surface in region 5. To decide between these two possibilities, an electrode was potentiostatically oxidized at -800 mV (vs. SCE) for 24 h in a pH 8 solution containing 10^{-3} M of sulphide; at a potential at which electrochemical oxidation to produce Fe^{III} phases will not occur. The Raman spectra collected after this procedure exhibited only the bands at 284 cm^{-1} and 208 cm^{-1} expected for nanocrystalline mackinawite, Fig. 7(d). The location of the band due to the symmetrical stretching mode of FeS (283 cm^{-1}) and the absence of bands for partially oxidized mackinawite, elemental S, and Fe^{III} oxides, confirmed that air oxidation during electrode transfer to the spectrometer was avoided. Since the same analytical procedure was used in all Raman analyses, the features observed in the spectra recorded after PDS, Fig. 7(a–c), indicate the electrochemical formation of sulphur and Fe^{III}oxides.

3.6. Surface analyses after potentiostatic oxidations

Fig. 8 shows current vs. time plots, on a logarithmic scale, recorded in solutions containing 10^{-4} M and 10^{-3} M of sulphide at -0.55 V; i.e., in the later stages of region 4 and/or the early stages of region 5 (as defined in Fig. 2). At pH 10, Fig. 8(a), the current is initially high (> 1 mA/cm^{-2}) and independent of time, before decreasing as expected if a current-inhibiting film was formed. Subsequently, the log of the current decreases approximately linearly at a sulphide concentration of 10^{-4} M to a value in the region of 1 μA/cm^{-2}, a commonly observed signature for the growth of a passivating layer. Identical behavior is observed at the higher sulphide concentration indicating that the decrease in current is independent of concentration as expected if the current is controlled by the rate of formation of a passivating oxide. Noticeably, the current recorded at longer times at the sulphide concentration of 10^{-3} M maintains a value of ≥ 10 μA/cm^{-2}, consistent with the expectation that passivity would become progressively more difficult to maintain, even at pH 10, due to the chemical instability of Fe^{III} surface states in the presence of sulphide. At the two lower pH values, Fig. 8(b and c), this longer-term decrease in current is interrupted by an increase, the extent of which increases as the sulphide concentration is increased and as the pH is decreased indicating the occurrence of reactions involving sulphide. This is particularly marked at pH 8, Fig. 8(c), and consistent with the CVs, Fig. 3, which showed that any attempt to form a passive layer was thwarted by film breakdown at this pH. The large fluctuations in current at the two lower pH values for the sulphide concentration of 10^{-3} M indicate the films formed are physically unstable.

Fig. 9 shows Raman spectra recorded on the electrodes after potentiostatic oxidation at -0.55 V in 10^{-4} M of sulphide at pH 10, when a passive film was formed, and in 10^{-3} M of sulphide at pH 9 when film

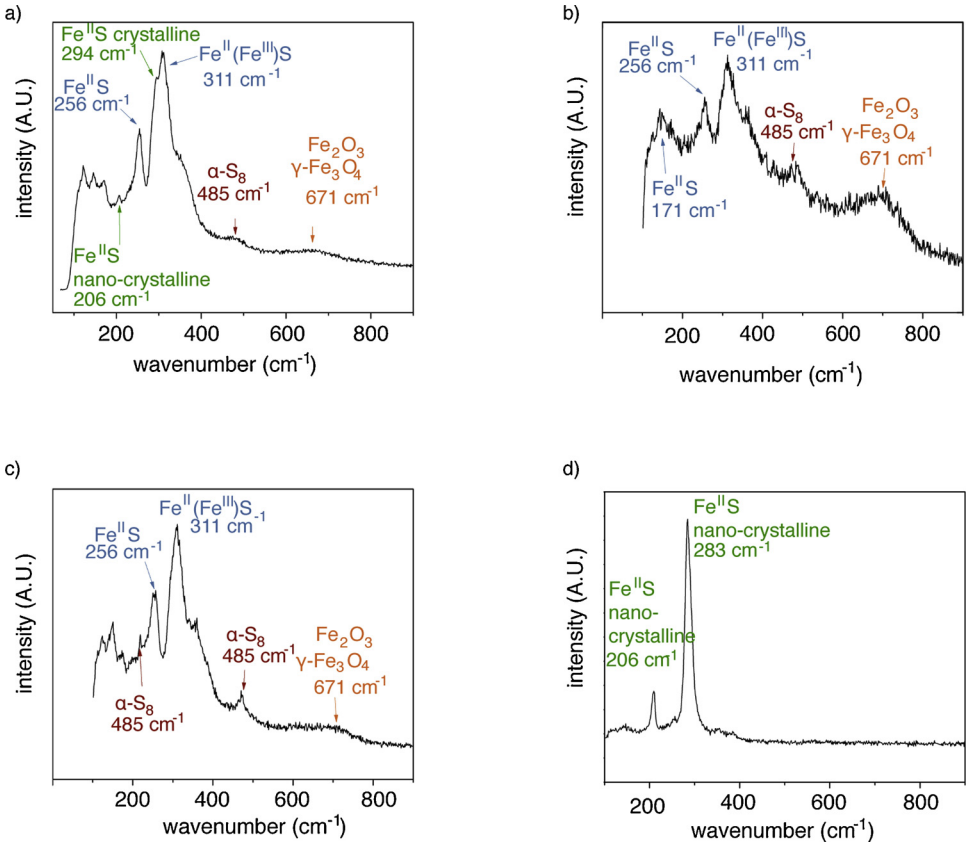

Fig. 7. Raman spectra recorded on a carbon steel electrode after poteniodynamic scans from -1.1 V to -0.4 V in a solution containing 10^{-3} M [SH-] and 0.2 M [CO_3^{2-}/HCO_3-] under anoxic conditions: a) pH 10, b) pH 9; c) pH 8. Raman spectra recorded after potentiostatic oxidation at -0.8 V vs. SCE for 12 h in a 0.2 M [CO_3^{2-}/HCO_3-] solution (pH 8) solution followed by the addition of 10^{-3} M [SH-] for 12 h. Red - α-S_8; blue - partially oxidized FeS; green - nano-crystalline FeS; brown - Fe_3O_4 and y-Fe_2O_3. (For interpretation of the references to colour in this figure legend, the reader is referred to the web version of this article).

breakdown and the formation of a current-inhibiting, but non-passive, layer was formed. At pH 10, the peak doublet (~675 cm^{-1} and ~720 cm^{-1}) confirms the presence of Fe_3O_4/γ-Fe_2O_3, as would be expected for the formation of a passive film. The broad peaks in the 300 - 600 cm^{-1} range are difficult to assign, but the peak at ~315 cm^{-1} could indicate the presence of partially oxidized mackinawite. A very broad band between 1250 cm^{-1} and 1600 cm^{-1} superimposed on a steeply increasing background signal (not shown) confirms the presence of an

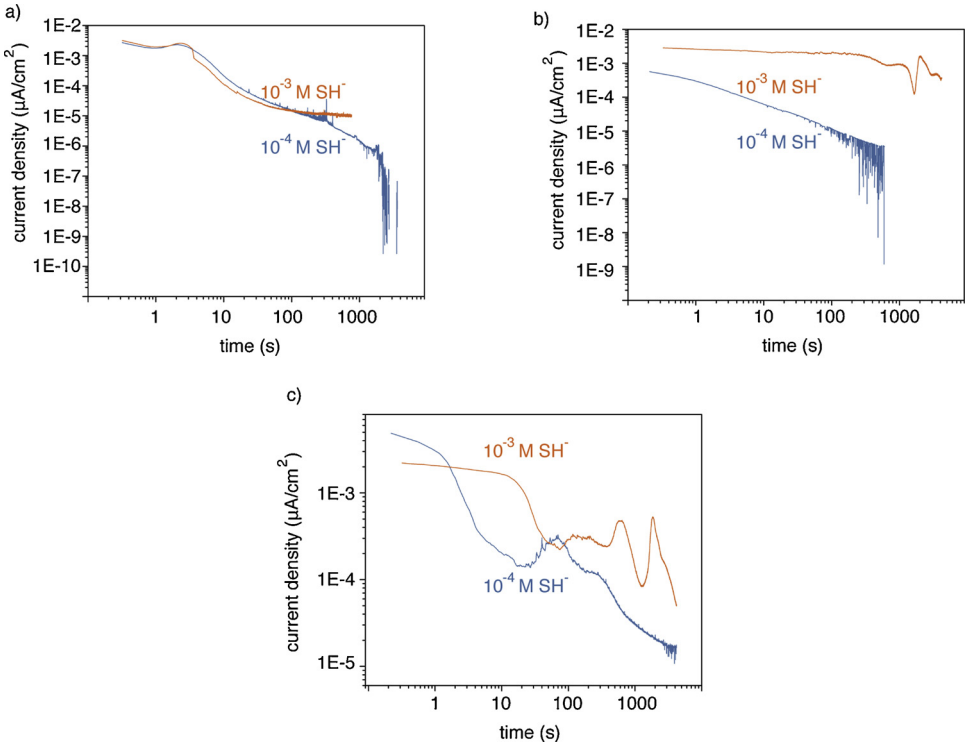

Fig. 8. Current-time logarithmic plots recorded on carbon steel polarized at -0.55 V vs. SCE in a 0.2 M CO_3^{2-}/HCO_3- solution containing different [SH-]: a) pH 10; b) pH 9; c) pH 8.

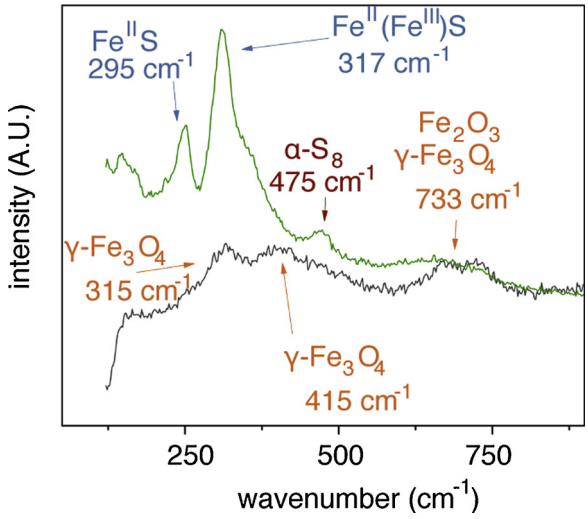

Fig. 9. Raman spectra recorded on carbon steel after anodic oxidation at -0.55 V for 70 min in a 0.2 M CO_3^{2-}/HCO_3-, solution containing either 10^{-4} M SH- (pH 10) (black) or 10^{-3} M [SH-] (pH 9) (green). Red: α-S_8, blue: partially oxidized FeS, green: nono-crystalline FeS, orange: Fe_3O_4 and γ-Fe_2O_3. (For interpretation of the references to colour in this figure legend, the reader is referred to the web version of this article).

Fe_3C residue which is detectable since the surface films are thin. The SEM micrographs in Fig. 10(a and b) confirm the presence of only a thin film (the original polishing lines remain visible in (a)) although the micrograph at a higher magnification, Fig. 10(b), indicates the film is crystalline on the nanometer scale which could indicate the presence of mackinawite.

At pH 9 and a sulphide concentration of 10^{-3} M, when the log I vs. log t plot exhibited higher currents associated with film breakdown, Fig. 8(b), the Raman spectrum is very similar to those observed after PDS experiments, Fig. 7, confirming that the breakdown of any Fe^{III} oxide film via the reaction sequence (8) to (15) leads to the formation of thick partially oxidized mackinawite, sulphur, and γ-Fe_2O_3/Fe_3O_4 layer. The SEM micrographs in Fig. 10(c and d) confirm the presence of a thick, easily detachable film of mackinawite comprised of nano-particulate clusters.

The initial formation of nanocrystalline mackinawite followed by its conversion to crystalline mackinawite with the process occurring more readily at high sulphide concentrations is consistent with published evidence indicating that the formation of the nanocrystalline precipitate occurred via the initial formation of $Fe(SH)_2$ which then condenses to yield FeS clusters (possibly Fe_2S_2) [32,47]. Since the structure of these clusters is similar to the basic structural component of mackinawite they act as precursors to the formation of nanocrystalline mackinawite [48]. These clusters form rapidly as the dominant form at high $[Fe^{2+}]$ and $[SH^-]$ with the first formed precipitate ~ 2.2 ± 1.7 nm in particulate size [32].

This offers a potential explanation for the observations in CVs that FeS formed at low sulphide concentrations and low dissolved $[Fe^{2+}]$ are retained on the electrode surface in a reducible form while those formed at high concentrations are not, Fig. 3. At low concentrations the formation of $Fe(SH)_2$ complexes leads to the relatively slow formation of a coherent and electrochemically reducible FeS layer on the steel surface. By contrast high concentrations lead to rapid progression from $Fe(SH)_2$ to FeS clusters (with stoichiometries up to $Fe_{150}S_{150}$) and the formation of lightly adherent and/or detached nanoparticles.

3.6.1. X-ray photoelectron spectroscopy

XPS spectra were recorded for the S 2p (160 eV–175 eV) and Fe $2p_{3/2}$ (705 eV–725 eV) regions after PDS experiments to a potential limit of -0.4 V (region 5) in a 0.2 M HCO_3^-/CO_3^{2-} solution containing a sulphide concentration of 10^{-3} M at pH 8 and pH 9. Spectra recorded at pH 10 were not analyzed in detail since the steel surface was readily passivated, as discussed above, and only minor amounts of sulphur species were observed. The spectra recorded at the two lower pH values are shown in Fig. 11. The parameters required to fit the S 2p spectra were taken from Pratt et al. [49]. The basis for fitting the Fe 2p spectra was developed by Gupta and Sen [50] and Grosvenor et al. [51] and the parameters used to fit the spectra in this study were developed by

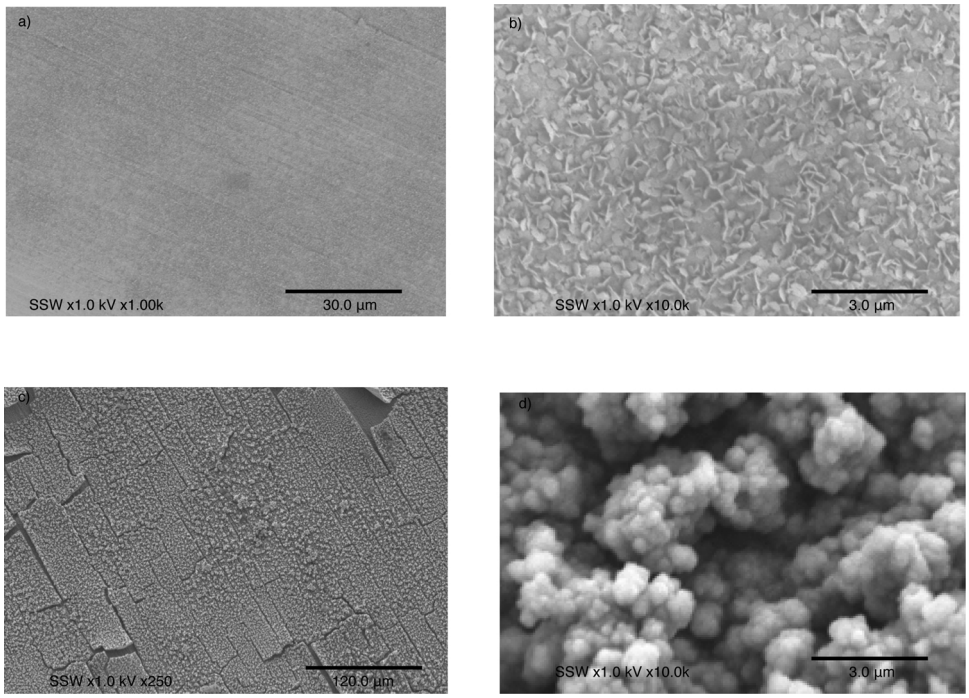

Fig. 10. (a,b) SEM images recorded after potentiostatic oxidation at -0.55 V for 70 min in a 0.2 M CO_3^{2-}/HCO_3-solution containing 10^{-4} M [SH-] (pH 10). (c,d) SEM images recorded after potentiostatic oxidation at -0.55 V for 70 min in a 0.2 M CO_3^{2-}/HCO_3- solution containing 10^{-3} M [SH-] (pH 9).

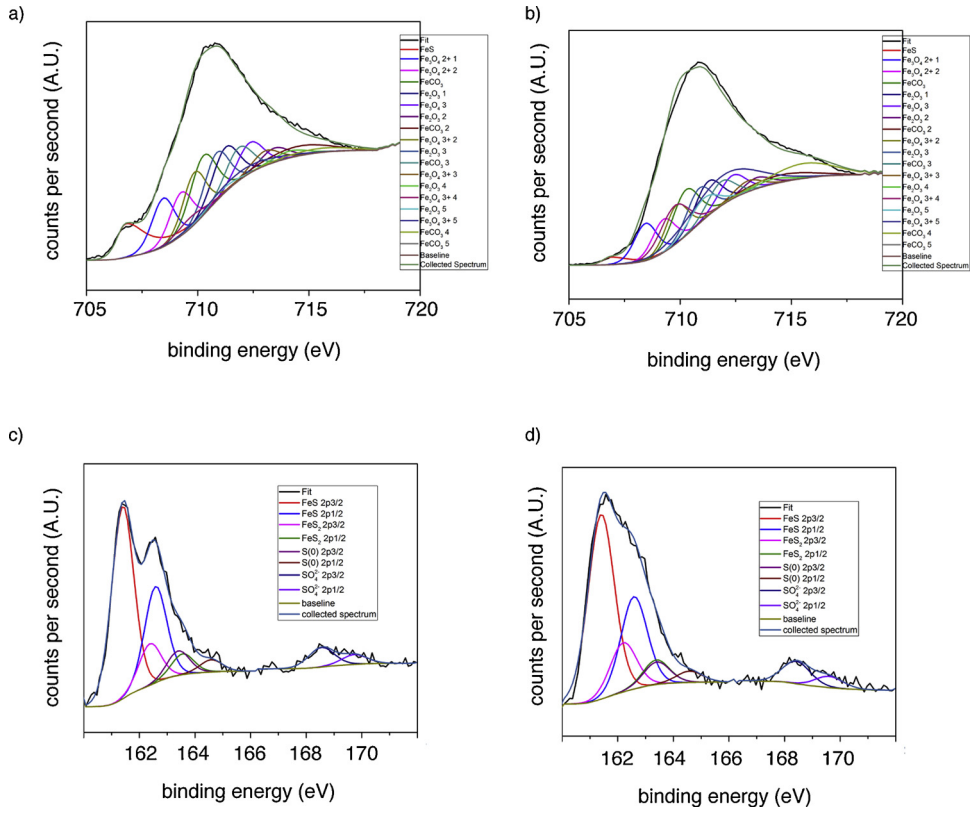

Fig. 11. High resolution deconvoluted XPS spectra for the S 2p peak recorded after PDP scan from -1.1 V to -0.4 V in a 0.2 M CO_3^{2-}/HCO_3- solution containing 10^{-3} M [SH-] at a) pH 9, b) pH 8. High resolution deconvoluted spectra for the Fe 2p3/2 XPS peak in the same solution c) pH 9, d) pH 8.

Biesinger et al. [52].

The S 2p spectra, Fig. 11(a and b), show the presence of sulphur species ranging from sulphide (S^{2-}), (161.2 eV), polysulphide (S_2^{2-}) (162.5 eV), elemental sulphur (164.3 eV) and sulphate (SO_4^{2-}) (168.7 eV) with the relative peak areas being similar at both pH values. The observation of oxidized species is consistent with the Raman spectra and the electrochemical behavior and demonstrates that the surface remains active, rather than passive in region 5.

Although the extent of reaction cannot be assessed on the basis of XPS analyses of the top ~ 5 nm of the surface deposit, the observation of oxidized S species confirms that the reaction sequence (11) to (14) proceeds, to some degree through, the sequence,

$$SH^- \rightarrow S_2^{2-} \rightarrow S_2O_3^{2-} \rightarrow SO_4^{2-} \quad (17)$$

with elemental sulphur produced by the reaction between polysulphide and thiosulphate. Whether sulphate exists as $FeSO_4$ or Na_2SO_4 is uncertain, since sodium was detected in the XPS survey spectra.

The deconvoluted Fe $2p_{3/2}$ are shown in Fig. 11(c) and d). The peak/shoulder at ~ 706.6 eV would normally be attributed to metallic Fe, [52] but is assigned to FeS [49] since the mackinawite deposit is too thick for the substrate steel to be detected. Deconvolution of the spectra demonstrates the presence of Fe_3O_4, Fe_2O_3, $FeCO_3$ (siderite) as expected based on the Raman spectra. Given the presence of polysulphide in the S 2p spectra, pyrite (FeS_2) may also be present, with a strong, near symmetrical peak at 707 eV and a distinct high energy tail extending to about 712 eV [53]. However, no improvement to the spectral fits, Fig. 12(c and d) could be achieved by including such a contribution. The inclusion of a contribution from $FeCO_3$ would not be unexpected since the ability of HCO_3^- to compete with sulphide in complexing soluble Fe^{2+} increases as the pH decreases [32]. The absence in the Raman spectra of the characteristic peak at 1082 cm^{-1} for $FeCO_3$ and previous work which shows siderite is not a major corrosion product under similar conditions suggests that only minor amounts are

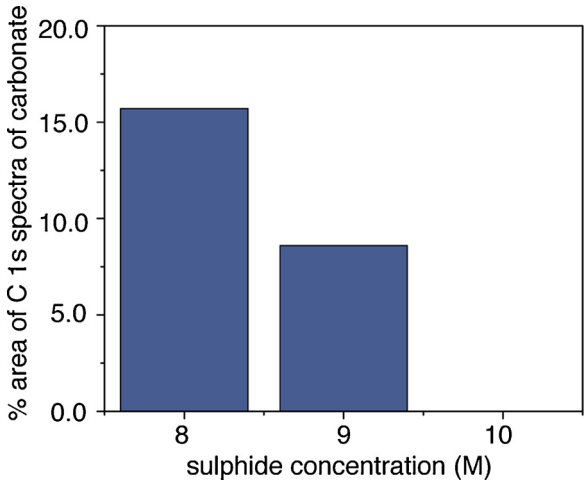

Fig. 12. relative amounts of carbonate determined from high resolution C 1s XPS spectra recorded after a PDP from -1.1 V to -0.4 V in a 0.2 M CO_3^{2-}/HCO_3 containing 10^{-3} M [SH-] as a function of pH.

present within the mackinawite deposit [54,55].

The presence of carbonate on the surface is confirmed by deconvolution of the C 1s spectrum (not shown) using the parameters taken from Beamson et al. [56]. Although carbonate could be present as Na_2CO_3 precipitated in the deposit during drying, the Fe 2p spectra confirm its presence in association with Fe^{2+}. The observed increase in the amount of carbonate in the surface as the pH was decreased, as seen in Fig. 12, was consistent with the calculations of Rickard and Luther [32]. The amount of carbonate present also increases as sulphide concentration is increased (not shown). Since both bicarbonate and sulphide concentration increase the rate of production of Fe^{2+},

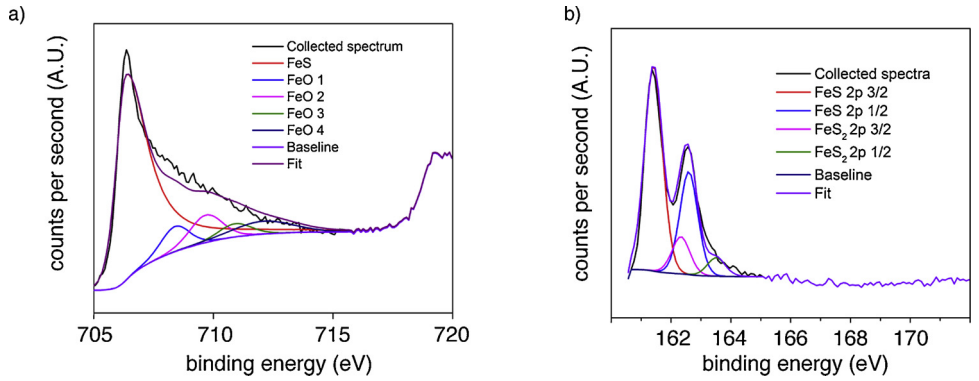

Fig. 13. High resolution spectra for the a) Fe 2p 3/2 and b) S 2p XPS peaks recorded on a spectra of steel electrode after potentiostatic oxidation at -800 mV for 24 h in a solution of 0.2 M CO_3^{2-}/HCO_3-, pH 8 for 12 h followed by the addition of 10^{-3} M [SH-] for the subsequent 12 h.

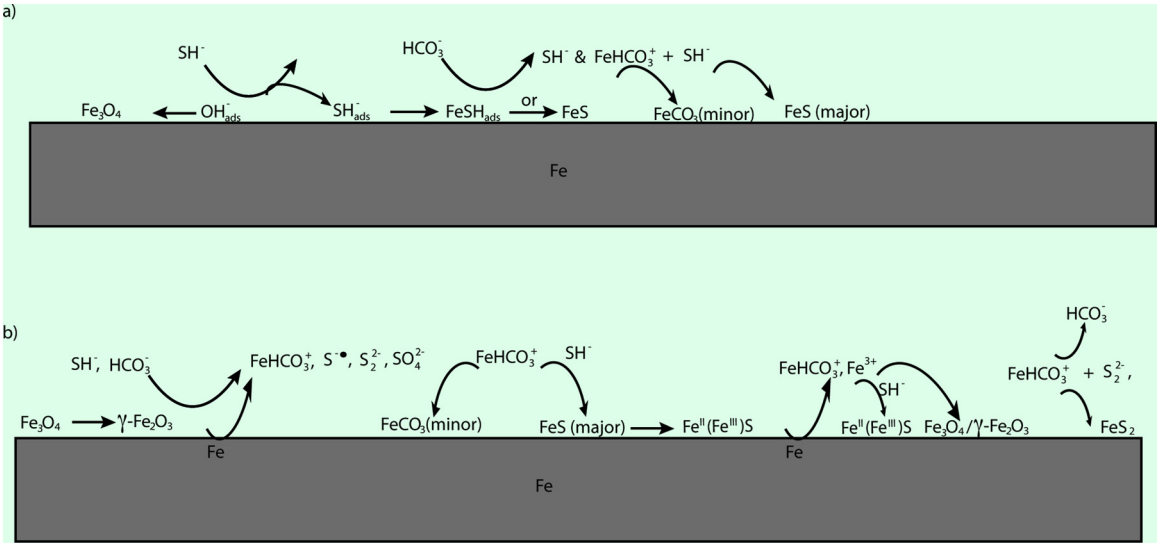

Fig. 14. Schematic representation of the mechanism of sulphide breakdown of the passive layer on iron oxides in a) regions 1 and 2, b) regions 3,4,5 (as defined in Figs. 1 and 2).

bicarbonate via reactions (6) and (9) and sulphide via reaction (9) and the reaction sequence (11) to (14), this is not unexpected.

Since XPS is a surface sensitive technique there remains the possibility that, despite the precautions taken, atmospheric oxidation could account for the observation of oxidized species and Fe^{III} states in the surface of the mackinawite deposit. To confirm that these oxidized states are produced either by the reaction sequence (11) to (14) or electrochemically when the potential is in region 5, an electrode was potentiostatically oxidized at -800 mV (vs. SCE) in a solution containing 0.2 M HCO_3^-/CO_3^{2-} (pH 8) for 12 h. After 12 h, sulphide was added to yield a solution with a sulphide concentration of 10^{-3} M and the potentiostatic experiment continued for a further 12 h with the current increasing from ~ 2 μA.cm^{-2} to ~ 9 μA.cm^{-2}. Under these conditions, Fe^{III}-containing surface states should not be formed precluding the occurrence of the reaction sequence (11) to (14) to produce oxidized sulphur species and the electrochemical formation of Fe^{III}-containing oxides. Fig. 13 shows the S 2p and Fe $2p_{3/2}$ spectra recorded on completion of this experiment after transfer of the electrode to the spectrometer using the procedure adopted in all analyses. In the S 2p spectrum no elemental sulphur or sulphate was observed although a minor contribution from polysulphide could be present. In the Fe $2p_{3/2}$ spectrum the dominant contribution was from FeS which is expected since mackinawite would be formed. Minor contributions from $Fe^{II}O$ species were observed, as expected during the pre-oxidation at -800 mV, but no trace of Fe^{III} surface species was detected. Despite the observation of polysulphide in the S 2p spectrum, no obvious signature for either elemental sulphur or sulphate was observed. This experiment demonstrates that the transfer of electrodes from the cell in the anaerobic chamber to the spectrometer avoided any significant atmospheric oxidation, confirming that the oxidized S species and Fe^{III}-containing oxides observed after PDS experiments were a consequence of the reaction sequence (11) to (14) and electrochemical processes in potential region 5.

4. Proposed mechanism

In the absence of sulphide, the anodic dissolution of carbon steel initiates with the adsorption of hydroxide on the steel surface and progresses with increasing potential through the anodic oxidation sequence (10). The extent of anodic dissolution as $FeHCO_3^+$ increases as the carbonate concentration increases and the pH decreases from 10 to 8. At pH 10 and pH 9, passivity can be maintained at positive potentials. However, at pH 8, when the pH is no longer buffered by the HCO_3^-/CO_3^{2-} equilibrium, film breakdown and dissolution of Fe^{3+}, followed by hydrolysis, leads to a decrease in pH and the loss of passivity.

When sulphide is present, even a low sulphide concentration can displace OH_{ads}^- from the steel surface. At pH 10, the threshold sulphide concentration is less than or equal to 10^{-6} M and lower, but undetermined at pH 8 and pH 9. At low potentials (regions 1 and 2), SH_{ads}^- interferes with the reaction sequence of $Fe(OH)_2$ to Fe_3O_4 by catalyzing anodic dissolution (as $FeHCO_3^+$), as illustrated in the schematic,

Fig. 14(a). Although not investigated in detail in this study, an increase in the surface concentration of dissolved $FeHCO_3^+$ would lead to the precipitation of FeS (mackinawite) and possibly $FeCO_3$ (siderite).

At more positive potentials, when the steel attempts to form Fe_2O_3 (region 3), the instability of Fe^{III} in the presence of sulphide prevents passivation by reducing Fe^{III} to Fe^{II}, which dissolves as $FeHCO_3^+$ and forms sulphide radicals ($S^{\cdot -}$), leading to the further reduction of Fe^{III} and the formation of elemental sulphur, polysulphide and eventually small amounts of sulphate, as illustrated schematically in Fig. 14(b). This reduction of Fe^{III} leads to reactivation of the steel surface and accelerated release of $FeHCO_3^+$ and its conversion by reaction with aqueous sulphide to yield insoluble mackinawite (FeS). Since polysulphides are also present the formation of pyrite is also possible although apparently not extensively. In addition, the deposition of siderite ($FeCO_3$) becomes possible but is also not extensive.

At pH 10, when buffering by HCO_3^-/CO_3^{2-} is effective, this reactivation of the steel surface is temporary with passivation by Fe_3O_4/γ-Fe_2O_3 being achieved at sufficiently positive potentials (region 5). At the lower pH values, the surface remains active with the direct oxidation of mackinawite yielding the partially oxidized form ($Fe^{II}(Fe^{III})S$). In addition, the electrochemical formation of Fe^{3+} leads to the electrochemical formation on the steel surface of a non-passivating layer comprised of small amounts of Fe_3O_4/γ-Fe_2O_3 and copious amounts of FeS (formed by the reduction of Fe^{3+} by sulphide) much of which is in particulate form and detached from the steel surface.

5. Summary and conclusions

The electrochemical dissolution of steel in the presence of HCO_3^-/CO_3^{2-} and sulphide is dependent on the [HCO_3^-/CO_3^{2-}], [SH^-], and pH. The presence of sulphide destabilizes the formation of Fe^{II}/Fe^{III}oxides by competing for surface adsorption sites on Fe and by simultaneously reducing Fe^{III} to Fe^{II}.

- Small concentrations of sulphide ($\leq 10^{-6}$M) catalyze the anodic dissolution of steel in carbonate solutions.
- Fe^{III} oxides are unstable in the presence of sulphides, even at low concentrations, and are reduced to $FeHCO_3^+$ species. The accompanying oxidation of sulphide leads to the formation of elemental sulphur, polysulphides, and small amounts of sulphate.
- The passivity of steel (by γ-Fe_2O_3) only appears achievable at high pH ($\geq$ 10) when the effective HCO_3^-/CO_3^{2-} buffering prevents local acidification. For pH values less than or equal to 9 active behavior prevails.
- The dominant FeS formed is mackinawite, which can form either compact surface films (slow growth) or nanoparticulate deposits with many detached from the steel surface (rapid growth).
- The presence of polysulphides can lead to pyrite (FeS_2) formation.

Authorship contribution

D.W. Shoesmith and J.J Noël supervised the project. M. Goldman designed the experimental procedures, performed electrochemical experiments and surface analysis and interpreted results. C. Tully performed electrochemical experiments and edited the manuscript.

Data availability

The raw and processed data required to reproduce these findings cannot be shared at this time as the data also forms part of an ongoing study.

CRediT authorship contribution statement

Maxwell Goldman: Writing - original draft, Conceptualization, Methodology, Investigation. **Claire Tully:** Investigation, Writing - review & editing, Validation. **James J. Noël:** Writing - review & editing, Supervision. **David W. Shoesmith:** Writing - review & editing, Supervision.

Declaration of Competing Interest

The authors declare that they have no known competing financial interests or personal relationships that could have appeared to influence the work reported in this paper.

Acknowledgements

The authors would like to thank Surface Science Western for access to their analytical instruments. The project was funded by an Canadian Natural Sciences and Engineering Research Council (NSERC) Discovery grant.

Appendix A. Supplementary data

Supplementary material related to this article can be found, in the online version, at doi:https://doi.org/10.1016/j.corsci.2020.108607.

References

[1] R.C. John, W.C. Fort, Petroleum industry: corrosion, in: K.H.J. Buschow, R.W. Cahn, M.C. Flemings, B. Ilschner, E.J. Kramer, S. Mahajan, P. Veyssière (Eds.), Encyclopedia of Materials: Science and Technology, Elsevier, Oxford, 2001, pp. 6840–6842.
[2] J. Liang, G. Fredine, M. Holm, Y. Li, Effectiveness of shorter corrosion ILI Re-inspection interval with varied ILI technologies: finding the unexpected high corrosion growth rate of external corrosion and MIC on tape lines, Corrosion 2018, NACE International, Phoenix, Arizona, USA, 2018, p. 15.
[3] F. Xie, X. Li, D. Wang, M. Wu, D. Sun, Synergistic effect of sulphate-reducing bacteria and external tensile stress on the corrosion behaviour of X80 pipeline steel in neutral soil environment, Eng. Fail. Anal. 91 (2018) 382–396.
[4] X. Zhang, W. Xu, D.W. Shoesmith, J.C. Wren, Kinetics of H2O2 reaction with oxide films on carbon steel, Corros. Sci. 49 (12) (2007) 4553–4567.
[5] W. Xu, K. Daub, X. Zhang, J.J. Noel, D.W. Shoesmith, J.C. Wren, Oxide formation and conversion on carbon steel in mildly basic solutions, Electrochim. Acta 54 (24) (2009) 5727–5738.
[6] P. Refait, J.A. Bourdoiseau, M. Jeannin, D.D. Nguyen, A. Romaine, R. Sabot, Electrochemical formation of carbonated corrosion products on carbon steel in deaerated solutions, Electrochim. Acta 79 (2012) 210–217.
[7] M. Saheb, D. Neff, L. Bellot-Gurlet, P. Dillmann, Raman study of a deuterated iron hydroxycarbonate to assess long-term corrosion mechanisms in anoxic soils, J. Raman Spectrosc. 42 (5) (2011) 1100–1108.
[8] P.H. Refait, M. Abdelmoula, J.M.R. GÉnin, Mechanisms of formation and structure of green rust one in aqueous corrosion of iron in the presence of chloride ions, Corros. Sci. 40 (9) (1998) 1547–1560.
[9] R. Guilbaud, M.W. White, S. Poulton, Surface charge and growth of sulphate and carbonate green rust in aqueous media, Geochim. Cosmochim. Acta 108 (1) (2013) 141–153.
[10] M.M. El-Naggar, Effects of Cl−, NO3− and SO42− anions on the anodic behavior of carbon steel in deaerated 0.50M NaHCO3 solutions, Appl. Surf. Sci. 252 (18) (2006) 6179–6194.
[11] G. Vatankhah, M. Drogowska, H. Menard, L. Brossard, Electrodissolution of iron in sodium sulfate and sodium bicarbonate solutions at pH8, J. Appl. Electrochem. 28 (2) (1998) 173–183.
[12] C.T. Lee, Z. Qin, M. Odziemkowski, D.W. Shoesmith, The influence of groundwater anions on the impedance behaviour of carbon steel corroding under anoxic conditions, Electrochim. Acta 51 (8–9) (2006) 1558–1568.
[13] C.T. Lee, M.S. Odziemkowski, D.W. Shoesmith, An in situ Raman-electrochemical investigation of carbon steel corrosion in Na2CO3 / NaHCO3, Na2SO4, and NaCl solutions, J. Electrochem. Soc. 153 (2) (2006) 33–41.
[14] Y. El Mendili, A. Abdelouas, J.-F. Bardeau, The corrosion behavior of carbon steel in sulfide aqueous media at 30°C, J. Mater. Eng. Perform. 23 (4) (2014) 1350–1357.
[15] H. Ma, X. Cheng, G. Li, S. Chen, Z. Quan, S. Zhao, L. Niu, The influence of hydrogen sulfide on corrosion of iron under different conditions, Corros. Sci. 42 (10) (2000) 1669–1683.
[16] M. Nordsveen, S. Nešić, R. Nyborg, A. Stangeland, A mechanistic model for carbon dioxide corrosion of mild steel in the presence of protective Iron carbonate films—part 1: theory and verification, Corrosion 59 (5) (2003) 443–456.
[17] T. Hemmingsen, H. Lima, Electrochemical and optical studies of sulphide film formation on carbon steel, Electrochim. Acta 43 (1–2) (1998) 35–40.
[18] D.W. Shoesmith, P. Taylor, M.G. Bailey, D.G. Owen, The formation of ferrous monosulfide polymorphs during the corrosion of Iron by aqueous hydrogen sulfide at 21°C, J. Electrochem. Soc. 127 (5) (1980) 1007–1015.
[19] D.W. Shoesmith, M.G. Bailey, B. Ikeda, Electrochemical formation of mackinawite

in alkaline sulphide solutions, Electrochim. Acta 23 (12) (1978) 1329–1339.
[20] D.W. Shoesmith, P. Taylor, M.G. Bailey, B. Ikeda, Electrochemical behaviour of iron in alkaline sulphide solutions, Electrochim. Acta 23 (9) (1978) 903–916.
[21] D.-p. Li, L. Zhang, J.-w. Yang, M.-x. Lu, J.-h. Ding, M.-l. Liu, Effect of H2S concentration on the corrosion behavior of pipeline steel under the coexistence of H2S and CO2, Int. J. Min. Metallur. Mat. 21 (4) (2014) 388–394.
[22] J. Vera, S. Kapusta, N. Hackerman, Localized corrosion of Iron in alkaline sulfide solutions: iron sulfide formation and the breakdown of passivity, J. Electrochem. Soc. 133 (3) (1986) 461–467.
[23] N. Sridhar, D.S. Dunn, A.M. Anderko, M.M. Lencka, H.U. Schutt, Effects of water and gas compositions on the internal corrosion of gas pipelines—modeling and experimental studies, Corrosion 57 (3) (2001) 221–235.
[24] B.W.A. Sherar, I.M. Power, P.G. Keech, S. Mitlin, G. Southam, D.W. Shoesmith, Characterizing the effect of carbon steel exposure in sulfide containing solutions to microbially induced corrosion, Corros. Sci. 53 (3) (2011) 955–960.
[25] E.B. Castro, J.R. Vilche, A.J. Arvia, Iron dissolution and passivation in K2CO3-KHCO3 solutions. rotating ring disc electrode and XPS studies, Corros. Sci. 32 (1) (1991) 37–50.
[26] J. Flis, T. Zakroczymski, Enhanced hydrogen entry in Iron at Low Anodic and low cathodic polarizations in neutral and alkaline solutions, Corrosion 48 (7) (1992) 530–539.
[27] M. Büchler, P. Schmuki, H. Böhni, T. Stenberg, T. Mäntylä, Comparison of the semiconductive properties of sputter-deposited Iron oxides with the passive film on Iron, J. Electrochem. Soc. 145 (2) (1998) 378–385.
[28] R.M. Cornell, U. Schwertmann, The Iron Oxides: Structure, Properties, Reactions, Occurrences and Uses, Wiley, 2006.
[29] M. Dos Santos Afonso, W. Stumm, Reductive dissolution of iron(III) (hydr)oxides by hydrogen sulfide, Langmuir 8 (6) (1992) 1671–1675.
[30] S.W. Poulton, M.D. Krom, R. Raiswell, A revised scheme for the reactivity of iron (oxyhydr)oxide minerals towards dissolved sulfide, Geochim. Cosmochim. Acta 68 (18) (2004) 3703–3715.
[31] T. Martino, J. Chen, Z. Qin, D.W. Shoesmith, The kinetics of film growth and their influence on the susceptibility to pitting of copper in aqueous sulphide solutions, Corros. Eng. Sci. Technol. 52 (1) (2017) 61–64.
[32] D. Rickard, G.W. Luther, Chemistry of iron sulfides, Chem. Rev. 107 (2) (2007) 514–562.
[33] M.P. Ryan, R.C. Newman, G.E. Thompson, An STM study of the passive film formed on Iron in borate buffer solution, J. Electrochem. Soc. 142 (10) (1995) L177–L179.
[34] M. Büchler, P. Schmuki, H. Böhni, Formation and dissolution of the passive film on Iron Studied by a light reflectance technique, J. Electrochem. Soc. 144 (7) (1997) 2307–2312.
[35] P. Schmuki, S. Virtanen, A.J. Davenport, C.M. Vitus, In situ X-Ray absorption near-edge spectroscopic study of the cathodic reduction of artificial Iron oxide passive films, J. Electrochem. Soc. 143 (2) (1996) 574–582.
[36] K. Yazdanfar, X. Zhang, P.G. Keech, D.W. Shoesmith, J.C. Wren, Film conversion and breakdown processes on carbon steel in the presence of halides, Corros. Sci. 52 (4) (2010) 1297–1304.
[37] J.A. Bourdoiseau, M. Jeannin, R. Sabot, C. Rémazeilles, P. Refait, Characterisation of mackinawite by Raman spectroscopy: effects of crystallisation, drying and oxidation, Corros. Sci. 50 (11) (2008) 3247–3255.
[38] G. Genchev, K. Cox, T.H. Tran, A. Sarfraz, C. Bosch, M. Spiegel, A. Erbe, Metallic, oxygen-containing reaction products after polarisation of iron in H2S saturated saline solutions, Corros. Sci. 98 (2015) 725–736.
[39] A. Boughriet, R.S. Figueiredo, J. Laureyns, P. Recourt, Identification of newly generated iron phases in recent anoxic sediments: 57Fe Mössbauer and microRaman spectroscopic studies, J. Chem. Soc. Faraday Trans. 93 (17) (1997) 3209–3215.
[40] S. Pineau, R. Sabot, L. Quillet, M. Jeannin, C. Caplat, I. Dupont-Morral, P. Refait, Formation of the Fe(II–III) hydroxysulphate green rust during marine corrosion of steel associated to molecular detection of dissimilatory sulphite-reductase, Corros. Sci. 50 (4) (2008) 1099–1111.
[41] E.B. Hansson, M.S. Odziemkowski, R.W. Gillham, Formation of poorly crystalline iron monosulfides: surface redox reactions on high purity iron, spectro-electrochemical studies, Corros. Sci. 48 (11) (2006) 3767–3783.
[42] A. Berner, Iron sulfides formed from aqueous solution at low temperatures and atmospheric pressure, J. Geol. 72 (3) (1964) 293–306.
[43] L. Benning, R. T Wilkin, H. L Barnes, Reaction pathways in the Fe–S system below 100°C, Chem. Geol. 167 (1-2) (2000) 25–51.
[44] S. Boursiquot, M. Mullet, M. Abdelmoula, J.M. Génin, J.J. Ehrhardt, The dry oxidation of tetragonal FeS1-xmackinawite, Physical Chemistry Minerals 28 (9) (2001) 600–611.
[45] R. Lennie, S. Redfern, E. Champness, C. Stoddart, P. Schofield, D. Vaughan, Transformation of mackinawite to greigite: an in situ X-ray powder diffraction and transmission electron microscope study, Journal of Earth and Planetary Materials 82 (3-4) (1997) 302–309.
[46] M. Mullet, S. Boursiquot, M. Abdelmoula, J.-M. Génin, J.-J. Ehrhardt, Surface chemistry and structural properties of mackinawite prepared by reaction of sulfide ions with metallic iron, Geochim. Cosmochim. Acta 66 (5) (2002) 829–836.
[47] S.M. Theberge, G.W. Luther Iii, Determination of the electrochemical properties of a soluble aqueous FeS species present in sulfidic solutions, Aquat. Geochem. 3 (3) (1997) 191–211.
[48] Mt. Wolthers, S.J. Van der Gaast, D. Rickard, The structure of disordered mackinawite, Am. Mineral. 88 (11-12) (2003) 2007–2015.
[49] A.R. Pratt, I.J. Muir, H.W. Nesbitt, X-ray photoelectron and Auger electron spectroscopic studies of pyrrhotite and mechanism of air oxidation, Geochim. Cosmochim. Acta 58 (2) (1994) 827–841.
[50] R.P. Gupta, S.K. Sen, Calculation of multiplet structure of core p -vacancy levels. II, Phys. Rev. B 12 (1) (1975) 15–19.
[51] A.P. Grosvenor, B.A. Kobe, M.C. Biesinger, N.S. McIntyre, Investigation of multiplet splitting of Fe 2p XPS spectra and bonding in iron compounds, Surf. Interface Anal. 36 (12) (2004) 1564–1574.
[52] M.C. Biesinger, B.P. Payne, A.P. Grosvenor, L.W.M. Lau, A.R. Gerson, R.S.C. Smart, Resolving surface chemical states in XPS analysis of first row transition metals, oxides and hydroxides: Cr, Mn, Fe, Co and Ni, Appl. Surf. Sci. 257 (7) (2011) 2717–2730.
[53] H.W. Nesbitt, G.M. Bancroft, A.R. Pratt, M.J. Scaini, Sulfur and iron surface states on fractured pyrite surfaces, Am. Mineral. 83 (9-10) (1998) 1067–1076.
[54] M. Odziemkowski, J. Flis, D.E. Irish, Raman spectral and electrochemical studies of surface film formation on iron and its alloys with carbon in Na2CO3/NaHCO3 solution with reference to stress corrosion cracking, Electrochim. Acta 39 (14) (1994) 2225–2236.
[55] M. Goldman, J.J. Noël, D.W. Shoesmith, Long-term sour corrosion of carbon steel in anoxic conditions, Corrosion 76 (3) (2020) 324–331.
[56] H. Hantsche, G. Beamson, D. Briggs (Eds.), High Resolution XPS of Organic Polymers, the Scienta ESCA300 Database, Wiley, 1992.